Ocean Dynamics (2011) 61:1967–1979
DOI 10.1007/s10236-011-0461-0

Characterization of ocean surface current properties from single site HF/VHF radar

Julien Marmain · Philippe Forget · Anne Molcard

Received: 7 January 2011 / Accepted: 17 June 2011 / Published online: 10 July 2011

Abstract Surface current mapping from HF/VHF coastal radars traditionally requires at least two distant sites. Vector velocities are estimated by combining the radial velocity components measured by the radars. In many circumstances (e.g., failures, interferences, logistics constraints), such a combination is not possible by lack of data from one station. Two methods are evaluated to get information on surface circulation from a single site radar: the Vectorial Reconstruction Method (VRM) for current vector mapping and the Vortex Identification Method (VIM) for detecting eddy-like structures. The VRM assumes a non-divergent horizontal surface current, and the VIM analyzes radial velocities and their radial and orthoradial gradients. These two methods are tested on modeled and measured data sets in the Northwestern Mediterranean Sea where both high-resolution ocean circulation model and radar campaigns are available. The VRM performance is strongly limited by the divergence-free hypothesis which was not satisfied in our real data. The VIM succeeded in detection of vortex in the Gulf of Lions and from an operating single site radar located on the Provence coasts in summer.

Keywords HF/VHF coastal radar · Single site radar · Stream function · Coastal eddies

Responsible Editor: Michel Rixen

This article is part of the Topical Collection on *Maritime Rapid Environmental Assessment*

J. Marmain (✉) · P. Forget · A. Molcard
Laboratoire de Sondages Electromagnétique de l'Environnement Terrestre (LSEET), UMR6017, CNRS/USTV,
Université du Sud Toulon Var,
BP 20132, 83957 La Garde Cedex, France
e-mail: julien.marmain@univ-tln.fr

1 Introduction

Coastal radar observations are relatively new data and have developed drastically in the last decade. This remote sensing technique has a large potential to describe surface current allowing high spatial and temporal resolution maps with broad spatial coverage (recently, Kaplan and Largier 2006; Shay et al. 2007; Yoshikawa et al. 2007; Shadden et al. 2009; Parks et al. 2009; Sentchev et al. 2009; Molcard et al. 2009; Allou et al. 2010; Kim 2010). The HF radar's range (12–30 MHz) can be as large as 100 km with a radial resolution of a few kilometers. Very High-Frequency (VHF) radars (30–50 MHz) are also used for higher radial resolution (up to 200 m) with a lower range (<20 km).

Current measurements are obtained from the Doppler shift of the first-order Bragg-resonant echoes originally described by Crombie (1955). The Bragg scattering designates the backscatter of electromagnetic waves from the ocean surface waves whose wavelength is half the wavelength of the radio wave. The current velocity component in the look direction of the radar is derived from the difference between the actual and the theoretical Bragg Doppler frequencies. The physics of current measurement by radar was first investigated by Stewart and Joy (1974). From the ensemble of the reflected radio waves during the measurement time window (usually 10–15 min) and from the Doppler spectrum of the resulting signal, the current velocity component along the radial direction can be measured. The drawbacks of the technique lie in the hardware cost, the frequency licenses, and the site finding, especially when the considered coast is irregular and steep or close to touristic and crowded regions.

As the current vector field results from the combination of radial current maps, at least two distant radars are needed. Different methods of combination exist. Leise

(1984) develops a vectorial method for a dual-site radar based on the direct combination of the radial velocities linearly interpolated on a prescribed grid. Lipa and Barrick (1983) describe an algorithm based on the least squares technique. Liu et al. (2007) developed an algorithm based on a non-divergent surface flow. Normal Mode Analysis (Lipphardt et al. 2000), Open Boundary Mode Analysis (Lekien et al. 2004; Kaplan and Lekien 2007), and variational interpolation (2dVar; Yaremchuk and Sentchev 2009) are more recent techniques producing smooth 2D current fields.

The present study addresses the use of a single radar station for specifying surface circulation. This question arises when only one radar of a two-site network is available, e.g., because of a temporary failure of one radar or prior to the complete dual system installation. Reconstruction from a single site radar was attempted several years ago by Frisch and Leise (1981) using the equation of continuity and May et al. (1989) using the spaced antenna technique. More recently, OMA (Kaplan and Lekien 2007) and 2dVar (Yaremchuk and Sentchev 2009) techniques were also used for current field reconstruction in such a case.

We investigate here two complementary methods for extracting information from a single site radar. The first method uses the continuity equation and assumes that surface current is non-divergent. The second one is free of physical assumption and consists in identifying eddy-like current features from the analysis of the radial velocity patterns and its associated gradients. To evaluate these methods, several data sets have been used, all acquired in the Northwestern Mediterranean (NWM) with a Wellen Radar (WERA) (Gurgel et al. 1999) system, in the framework of national and international projects with specific scientific objectives. Besides, the methods have been evaluated using synthetic radial current data generated from the high-resolution ocean model Nucleus for European Models of the Ocean (NEMO) (Madec 2008).

The paper is organized as follows. Section 2.1 presents the two methods. Section 2.2 gives a description of the studied regions and the available experimental and modeled data. Section 3 presents applications to synthetic radial data sets from the NEMO model. Finally, Sect. 4 applies these methods to experimental data sets.

2 Methods and data

2.1 Reconstruction and identification methods

Two methods are evaluated to exploit the measurements from a single radar. The Vector Reconstruction Method (VRM) aims at calculating the horizontal current vector field. The Vortex Identification Method (VIM) consists in identifying eddy-like structures within the current field.

2.1.1 Vector reconstruction method

The VRM is based on the fundamental assumption that the divergence of the horizontal surface current is zero or at least negligible in such a way that:

$$\frac{\partial u}{\partial x}+\frac{\partial v}{\partial y}=0 \tag{1}$$

where u and v are the two velocity components in the x (east) and y (north) directions, respectively (Frisch and Leise 1981; Lipa and Barrick 1983; Liu et al. 2007). For radar measurements, surface current refers to a depth of approximately $\lambda/8\pi$, where λ is the radio wavelength, being typically equal to 0.75 m at 16 MHz and 0.27 m at 45 MHz (Stewart and Joy 1974). Considering the 3D incompressibility of sea water, Eq. 1 means that the vertical gradient of the vertical velocity is negligible at the surface.

Equation 1 writes in polar coordinates:

$$\frac{\partial(rV_r)}{\partial r}+\frac{\partial V_\theta}{\partial \theta}=0 \tag{2}$$

with $V_r \equiv u\cos\theta+v\sin\theta$ and V_θ the radial and orthoradial velocity components at distance r, respectively. When the radar is located in $r=0$, r and θ are the range and the azimuth of the radial velocity V_r (x, y) measured by the radar.

Introducing the stream function Ψ, we have

$$V_r=-\frac{1}{r}\left(\frac{\partial\Psi(r,\theta)}{\partial\theta}\right)_r \text{ and } V_\theta=\left(\frac{\partial\Psi(r,\theta)}{\partial r}\right)_\theta \tag{3}$$

The spatial differential of Ψ is

$$d\Psi=\left(\frac{\partial\Psi}{\partial r}\right)_\theta dr+\left(\frac{\partial\Psi}{\partial\theta}\right)_r d\theta=V_\theta dr-rV_r d\theta \tag{4}$$

which writes for a constant radar range

$$d\Psi=-rV_r d\theta \tag{5}$$

Equation 5 is a partial differential equation whose characteristic curves are circles centered around the radar location. Integration along each characteristic curve gives:

$$\Psi(r,\theta)=-r\int V_r d\theta+K \tag{6}$$

with K a constant of integration. It is then possible to compute the stream function from the radial component everywhere within the radar coverage, assuming Ψ is known at least at one point along every characteristic curve. Equation 6 was numerically solved using a first-order forward scheme. The computation is more accurate

using polar than cartesian coordinates, because the radar measurements are naturally provided in the polar form.

To obtain the current components on a predefined cartesian grid, Ψ was first linearly interpolated at each grid point and then used to calculate u and v by:

$$u = -\left(\frac{\partial \Psi}{\partial y}\right)_x \text{ and } v = \left(\frac{\partial \Psi}{\partial x}\right)_y \quad (7)$$

The cartesian grid can be any grid, e.g., the numerical model grid or the current vector maps grid of the experimental data (Sect. 2.2). Equation 7 is solved using a centered difference method.

In general, the constant K is not known. In practice, it is often possible to install a radar station in such a way that one edge of the coverage cone lies over an extended part of the land. It is reasonable to assume that the stream function, and therefore K, is constant in this region. In the absence of a continental coastline, another favorable situation is the presence of an island sufficiently extended along the range direction within the observation cone. In this case, Eq. 6 can be solved along the characteristic curves on each side of the island (where K can be assumed constant). When the radial extension of ground zones is too small compared to radar range resolution, typically 3 km in HF or 500 m in VHF, then Eq. 7 cannot be solved accurately. Similarly, the VRM process stops when the characteristic curves used for the reconstruction cross a small island resulting in shadowing effects on the reconstructed current field.

2.1.2 Vortex structure identification method from the radial velocity

This section shows the possibility of eddy-like structure identification from the radial velocity field and its radial and orthoradial derivatives. An idealized symmetrical vortex model (Martin et al. 2001) is used, defined by

$$V_\theta(r) = V_0 \frac{r}{r_0} \exp\left(\frac{1}{2}\left(1 - \frac{r^2}{r_0^2}\right)\right) \quad (8)$$

r_0 is the radius of the vortex, and V_0 is the maximum velocity occurring at $r=r_0$. In the example shown in Fig. 1, the vortex is cyclonic with r_0=5 km and V_0=0.5 $\mathrm{m\,s^{-1}}$. The theoretical radar is located at (20, 0).

In Fig.1a, the current field is superimposed to the radial velocity: V_r is positive-red (negative-blue) towards (away from) the radar, and the vortex appears as a dipole. Opposite values of V_r are distributed on both sides of the V_r zero line.

V_r first derivatives are sketched and analyzed on Fig. 1b and c. For the radial derivative $\mathrm{RD} = \frac{\partial V_r}{\partial r}$ (Fig. 1b), the vortex appears as a specific quadripole pattern with positive and negative lobes depending on the current rotation. The zero line of V_r corresponds to a zero line of RD. The other zero line of RD indicates local extrema of the radial velocity. In addition, the lobes closer to the radar are less extended than the distant ones.

Finally, the orthoradial derivative of V_r, $\mathrm{OD} = \frac{1}{r}\frac{\partial V_r}{\partial \theta}$, maps into a tripole (Fig. 1c). Zero lines of OD correspond to local extrema of the radial velocity.

This analysis shows that a symmetrical mesoscale vortex gives well-characterized signatures on the radial velocity maps and its radial and orthoradial derivatives. In theory, it may be possible to estimate the center of the vortex, its polarization (cyclonic or anti-cyclonic), its diameter, and its maximum current intensity from these signatures. However, the model is very basic and quite unrealistic. Hence, we can expect that accuracy of these estimates will be restricted by the likely deviations of real ocean structures from the model in terms of circular symmetry, current intensities, etc.… Moreover, the use of the VIM requires an ocean structure entirely embedded in the radar coverage.

In case of reasonable agreement of a real structure with the model, the accuracy of the estimates may be improved by a least-squares method fitting the measured radial currents to the model. However, focus here is more on the detection problem, i.e., to identify the presence of a vortex from radar measurements, than on the accurate determination of vortex characteristics. Improving the vortex feature accuracy is beyond the point of this study, so model parameters inversions have not been further studied.

The VIM method is based on an a priori expertise performed on the current fields from either experimental data or model simulations (Sect. 2.2). The training consists in detecting patterns by eye, similar to those sketched in Fig.1, on realistic current fields. This practice will allow the expert to apply the VIM to single radar data when total current field is not available.

The method performance and the confidence in the vortex detection are assessed through quality indices (r_{Vr}, r_{RD}, r_{OD}) applied to the V_r, RD, and OD maps, respectively. The index value is 0 (no detection), 1 (medium detection), or 2 (good detection) depending on the similarity between the observed and the theoretical patterns (Fig. 1). The greater the sum (S) of the indices, the better the confidence.

2.2 Data sets

2.2.1 Regions of study

The NWM basin (Fig. 2) is characterized by both a complex coastline and topography. The general circulation includes the Northern Current (NC), which is part of the cyclonic surface circulation, and a strong seasonal signal and mesoscale activity, such as gyres and fronts, mainly driven by the intense and highly variable wind regime

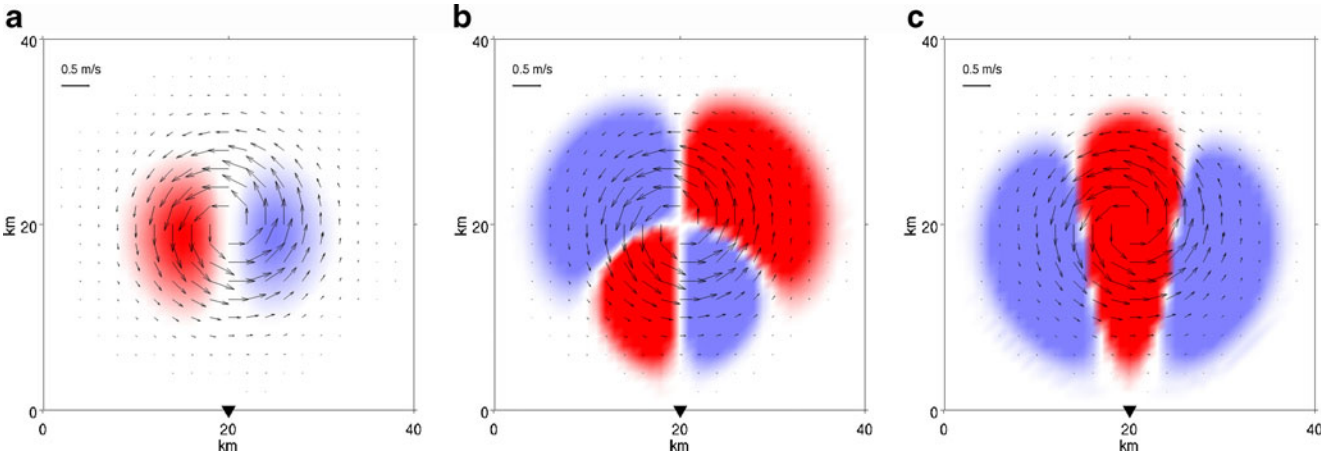

Fig. 1 Idealized symmetric vortex. *Colored patterns* correspond to **a** radial velocity field V_r, **b** radial derivative RD, and **c** orthoradial derivative OD of V_r. Radar is located at x=20 km and y=0 km (*black triangle*)

(Millot 1999; Sammari et al. 1995; Estournel et al. 2003; Petrenko et al. 2005; Flexas et al. 2002).

Four regions have been chosen in the NWM to evaluate the performance of the VRM and the VIM methods. Two of them have been surveyed during previous radar campaigns, one is currently instrumented with a single radar, and the other one is a planned future experiment.

The first region of study is the eastern part of the Gulf of Lions (Fig. 2, region 1). It was covered by a coastal radar during the Echanges côte-large dans le golfe du lion (ECOLO) campaign from June 2005 to January 2007 to study the NC intrusions on the gulf shelf. The great amount and the quality of surface current observations reveal interesting features, such as the NC meandering and variability, inertial circulation, and specific anti-cyclonic eddies (Allou et al. 2010; Schaeffer et al. 2011).

In the framework of the international program Maritime Rapid Environmental Assessment 2007 (MREA07) (Rixen et al. 2009), a 2-week experiment (June 2007) of continuous monitoring of the Gulf of La Spezia in the Ligurian Sea was carried out for dispersion studies (Molcard et al. 2009; Haza et al. 2010). An innovative concept of the experiment was the use of VHF WERA radars in quasi-operational mode. Current data from this small-scale basin (Fig. 2, region 2) will be considered.

The third region extends along the Provence coasts (Fig. 2, region 3). In the framework of national and international programs, a two-site radar system is planned for specific circulation studies in this region (Etude de la circulation côtière en zone provençale, ECCOP experiment). The local circulation, which is poorly documented, is mainly under the influence of the NC, controlled by a complex topography and wind regimes. The actual setting consists of a unique radar system recently installed (May 2010). The second site is expected to be operating by the end of 2011.

The experimental data sets used here are from the ECOLO, MREA, and ECCOP campaigns. High azimuthal resolution was achieved using a MUSIC processing method (Schmidt 1986; Lipa et al. 2006). For ECOLO and MREA, radial components were combined to map surface current vectors on a prescribed cartesian grid. Characteristics of the

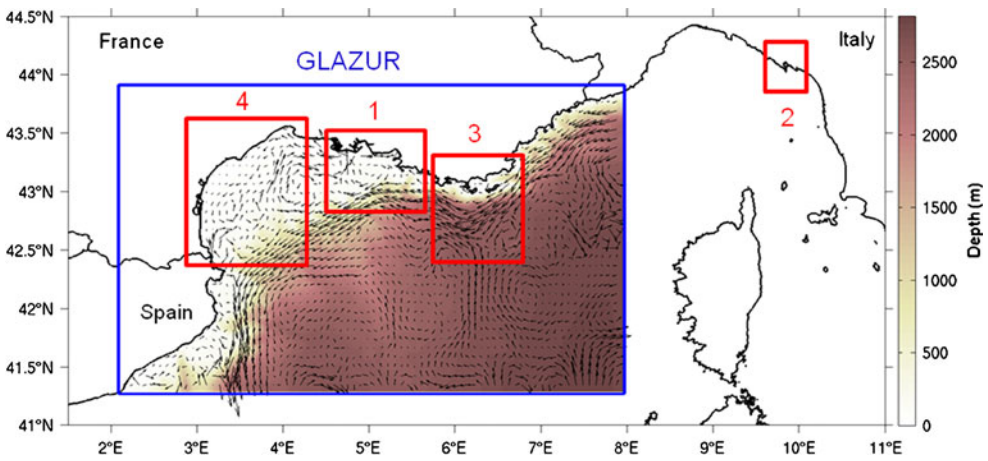

Fig. 2 Zone of study. Regions *1*, *2*, *3*, *4* (*red rectangles*) refer to ECOLO, MREA, ECCOP, and WGOL experiments in the text. The *blue rectangle* is the GLAZUR64 model domain. *Shaded color* represents the bathymetry used in GLAZUR64. *Black arrows* represent a particular surface current output from GLAZUR64, illustrating the significant mesoscale activity. Vectors are plotted every five grid points

radial and cartesian grids are given in Table 1 along with the relevant technical information. Detailed information on the implementation, the processing, and the available data can be found in Molcard et al. (2009) (MREA) and Forget et al. (2008), Allou et al. (2010), and Schaeffer et al. (2011) (ECOLO).

An additional region in the western part of the Gulf of Lions (WGOL, Fig. 2, region 4) will be considered to test the VRM method. This site, for which no radar data are currently available, is under investigation for future radar campaigns in the framework of national programs. In particular, the ongoing LATEX project (Hu et al. 2009, 2010) focuses on a specific submesoscale eddy recurrently observed by satellite images and appearing in numerical models. Radar observations will complement traditional in situ measurements to track this eddy and its evolution.

2.2.2 Model

A synthetic data set computed by a numerical model facilitates the assessment by producing smoothed and continuous current fields. The model used here, called GLAZUR64, is a recent configuration of the ocean general circulation model Nucleus for European Models of the Ocean (NEMO, Madec 2008). GLAZUR64 was developed to study the circulation in the NWM basin at high resolution (Ourmières et al. 2011). This NEMO configuration is an extension of a former version which was developed for the Gulf of Lions (Langlais et al. 2009) and covers the NWM from the Spanish coasts to the western part of the Ligurian Sea (Fig. 2). The vertical grid consists of 130 z levels with spacing varying from 1 m in the first 35 m to 30 m near the bottom in the Abyssal Plain (2,665 m). The horizontal resolution is 1/64° (about 1.25 by 1.25 km). Radiative conditions are used at the ocean open boundaries, and the boundary data are provided by MED16, a NEMO configuration with a horizontal resolution of 1/16° and 43 vertical z levels (Béranger et al. 2010). Atmospheric forcing is provided by the REMO model (Jacob et al. 2001) with a horizontal resolution of 1/6°, a vertical resolution of 24 layers up to 10 hPa, and a time resolution of 1 h. GLAZUR64 uses the bulk forcing approach to provide surface fluxes (Large and Yeager 2004). We use here numerical simulations for year 2001 as atmospheric forcing, and data for validation are available for this period. The model data set consists of fields of the ocean circulation averaged to 2 days for the considered year.

To be more realistic, a random noise was added to take into account the limited integration time, which involves a finite Doppler frequency resolution and then a finite velocity resolution, δV_r. Noise was uniformly distributed over an interval of 0.02 $\mathrm{m\,s^{-1}}$, which corresponds to an integration time of 10 min at a 16-MHz radar frequency. It should be noted that δV_r is a minimum estimate of the measurement error since there are other sources of noise in the radar current measurements such as the velocity variability within a radar cell and the statistical noise in the radar spectral data (Lipa 2003).

2.2.3 Experiments

To evaluate the VRM and the VIM, the regions described in Sect. 2.2.1 have been chosen because either radar or modeled data are available. Note that both data sets are not available simultaneously and that the regions are not all suitable for the application of both techniques. However, the goal here is to assess the methods according to the most suitable region for each of them and not to compare them.

Table 2 summarizes the experiments. The available radar data sets (regions 1–3 of Fig. 2) allow the testing of our methods when applied on different geographic locations and real dynamics. Surface currents of GLAZUR64 are used to generate synthetic radial components over regions 3 and 4.

Region 1 was chosen to test the VIM technique because radar-derived surface circulation evidenced a strong eddy activity. Since the radar coverage cones do not intersect the coastline, this data set is not adapted to the VRM technique. Current maps from the MREA campaign in region 2 did not evidence any well-pronounced eddy, so the VIM would be useless, and only the VRM is tested. In region 3, both model (year 2001) and radar data (year 2010) are used for VIM tests. The VRM is not applied due to the presence of small islands, leading to possible shadowing effects.

Table 1 Radar and data characteristics

	ECOLO	MREA	ECCOP
Central frequency (MHz)	16.15	45.25	16.15
Measurement depth ($\lambda/8\pi$) (m)	0.74	0.26	0.74
Range sampling (m)	3,000	300	3,000
Azimuthal resolution (°)	5	5	5
Radial accuracy δV_r ($\mathrm{m\,s^{-1}}$)	0.021	0.015	0.021
Mesh size (m)	5,000	250	–

Mesh size is that of the current vector grid. δV_r is the intrinsic accuracy of radial measurements, i.e., the velocity corresponding to the inverse of the sample duration

Table 2 Summary of the method used (VIM or VRM) in each region (Fig. 2) based on radar or modeled data

Region	1	2	3	4
Radar	VIM	VRM	VIM	–
Model	–	–	VIM	VRM

Moreover, surface current ground truth to evaluate the performance of the reconstruction method is not available. In region 4, only model data are available, and the VRM is tested. This region was chosen because of its smooth and continuous coastlines allowing a radar implementation which is well adapted to the method. The VIM could also have been used, but concerning the assessment of the method, it would not bring much to the results obtained in regions 1 and 3.

3 Application to modeled data

In this section, the VRM and the VIM techniques are evaluated in realistic environment as provided by GLAZUR64 simulations. From the simulated current field, considered as the ground truth, the radial components are computed by vector projection of the current on radial directions, as if they were directly observed by radars.

3.1 Vectorial Reconstruction Method in the Gulf of Lions

The VRM was applied to synthetic radar data produced by the model in region 4. The results obtained for the particular date of Fig. 3 are commented. The circulation shows a well-identified current along the coastline and two cyclonic eddies located at E3.60°–N42.70° and E3.95°–N43.05° (Fig. 3a). The surface current divergence (SCD) is superimposed on the modeled current. The SCD depicts a rather high spatial variability, observed throughout the year and corresponding to upwelling (positive sign) or downwelling (negative sign) areas. The SCD values range from -1.10^{-4} s^{-1} to 1.10^{-4} s^{-1}. A strong upwelling activity has been already reported in this region (Hua and Thomasset 1983; Millot 1990).

Figure 3c shows the norm of the vector speed difference, VSD, between the VRM (u_{VRM}, v_{VRM}) and the original (u, v) current fields according to:

$$\mathrm{VSD} = \sqrt{(u - u_{\mathrm{VRM}})^2 + (v - v_{\mathrm{VRM}})^2} \tag{9}$$

Reconstructed currents were computed from radial components affected by instrumental noise. Characteristic curves (Eq. 5) start from the coastline south of the radar. The VSD map displays an inhomogeneous and circular distribution. The instrumental noise is responsible for the quite pronounced differences between the adjacent characteristic curves, as seen on VSD maps corresponding to radial currents with and without additional noise (not shown). VSD values are low at the beginning of the characteristic curves, where SCD is generally low, and then vary along them with the divergence field.

The VSD value at a given position is found to be less dependent on the local SCD than on the cumulative sum of divergences (SCD_{cum}) from the beginning of the characteristic curves. There is a clear correlation between VSD and the absolute value of SCD_{cum} as illustrated in Fig. 4a (successive negative and positive SCD_{cum}) and Fig. 4b (negative SCD_{cum}). This goes further into the results of Frisch and Leise (1981) who observed a linear increase with distance along characteristic curves of the error due to the SCD. The instrumental noise has a low influence on such correlation properties.

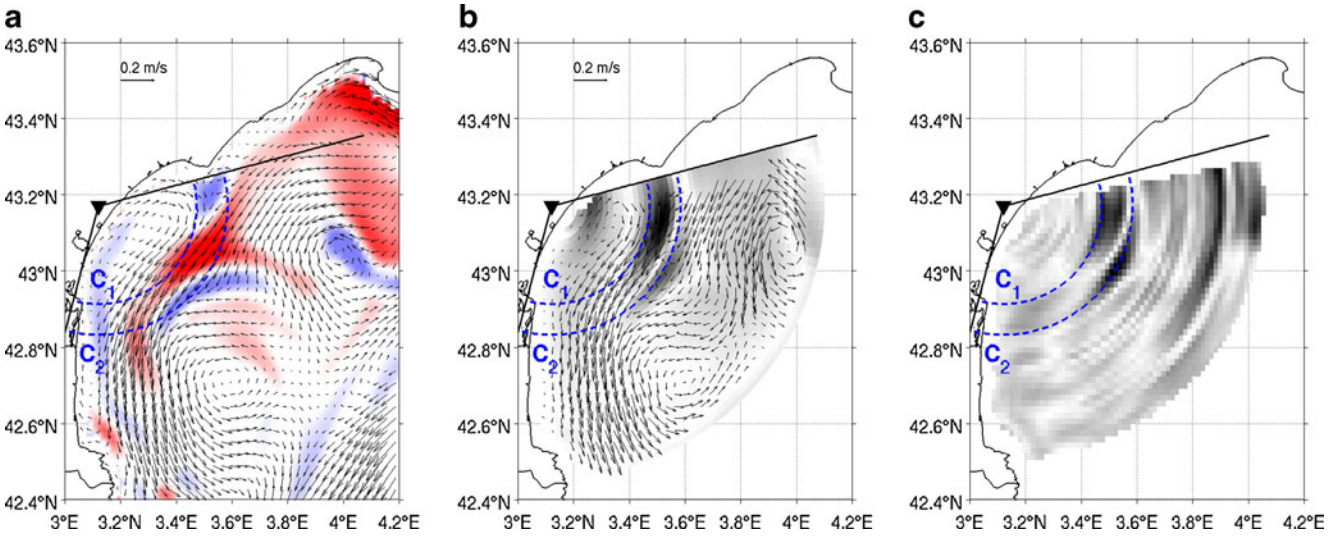

Fig. 3 Application of VRM on September 5, 2001. **a** Original surface current field (*arrows*) and divergence (*color*). *Color bar* from -5.10^{-6} s^{-1} (*blue*) to 5.10^{-6} s^{-1} (*red*). **b** Reconstructed (VRM) current (*arrows*) and cumulative sum of SCD (*gray scale* from 0 to 2.10^{-5} s^{-1}). **c** Norm of VSD between reconstructed and original fields. *Gray scale* from 0 ms^{-1} (*white*) to 0.1 ms^{-1} (*black*). *Blue lines* are characteristic curves for radar ranges 30 km (C1) and 46.5 km (C2). The *cone in black* is the theoretical radar coverage, and the *black triangle* is the radar location

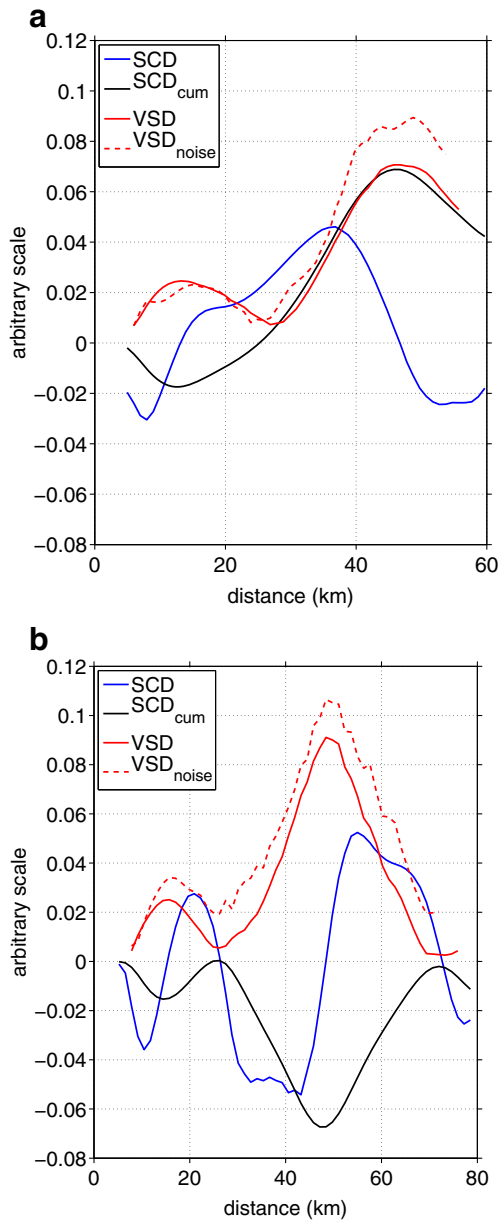

Fig. 4 Variation with distance along characteristic curve **a** C1 and **b** C2 of Fig. 3 of SCD×10^4 (per second), SCD_{cum}×10^3 (per second), and VSD (meters per second) with (*dashed line*) and without noise (*solid line*)

The reconstructed VRM current (Fig. 3b) reproduces quite well the coastal flow and the two eddies, in particular the center positions. Agreement is the most satisfactory in zones presenting the lowest SCD_{cum} values, e.g., south of 42.8° N.

These results are representative of what was obtained at other dates and are similar for a broad range of surface circulation patterns observed throughout the year. An important result is that, although reconstructed currents generally present realistic features, they can significantly differ from the original currents due to divergence effects. If no a priori information is available on the divergence properties, the method may be unsafe for vector field reconstruction. In practice, the VRM method should successfully work over areas of very low divergence. Selection of such zones could be done a priori from a statistical analysis of model circulation data to attribute confidence indices for VRM application. The model can only be used to check the applicability of VRM, if it is able to give realistic results on up- and downwelling, i.e., the divergence of the circulation.

3.2 Vortex identification method along the Provence coasts

The actual single radar implementation in region 3 should approximately enable the coverage shown in Fig. 5. The radar coverage intercepts the coast at the northern border, which is adapted for VRM use. However, the region includes many islands more or less extended which may introduce important discontinuities in the vector reconstruction (Sect. 2.1.1.). On the other hand, the simulation analysis revealed a significant mesoscale activity resulting in recurrent eddies over the year. Therefore, the VIM was preferred for this region.

Current vector maps in Fig. 5 show typical circulation features, such as the NC flowing from northeast to west, and vortices on its southern boundary. Note the bending of the NC south off the Porquerolles island (43.04° N–6.13° E) due to a steering bathymetric effect. The NC is present all over the year with a seasonal variability in terms of width, position, and current magnitude as described by both observations (Millot 1999; Petrenko 2003) and numerical results (André et al. 2005).

The statistical analysis of the GLAZUR64 2001 simulations gives an eddy occurrence of 30% (82 eddies over the 181 model outputs) with a very high seasonal variability (88% occurrence from November to April). Most eddies are observed in the southern part of the area where the depth is greater than 2,500 m (95%) and are cyclonic (89%). They are generally close to circular (mean eccentricity, 0.6) with a mean radius of 12 km (r_0 in Eq. 8). A similar mesoscale activity was reported in the Gulf of Lions (Flexas et al. 2002; Allou et al. 2010; Schaeffer et al. 2011).

The VIM results are illustrated in Fig. 5 depicting the spatial distribution of V_r and its derivatives RD and OD. Two vortices are detected in Fig. 5 with these distributions. The first one (V1) is circular and matches the idealized vortex model (Eq. 8) except for the circular homogeneity of the current intensity. Its signatures on radial currents and its derivatives feature the expected characteristic dipole (Fig. 5a), quadripole (Fig. 5b), and tripole (Fig. 5c) structures, including associated zero lines.

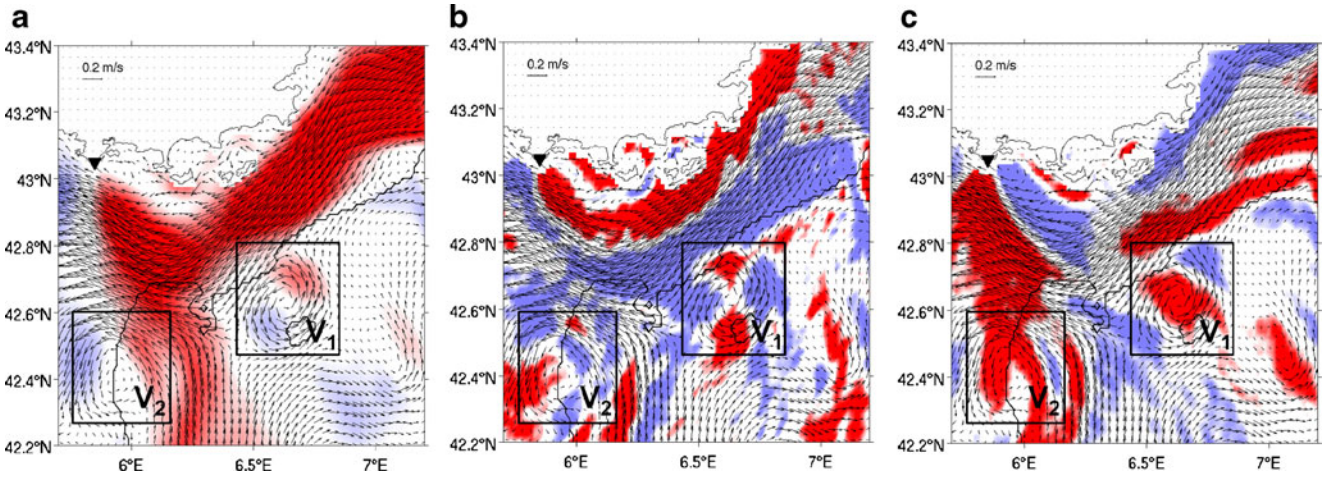

Fig. 5 Simulated map of **a** radial velocity field *Vr*, **b** radial derivative RD, and **c** orthoradial derivative OD of *Vr*, corresponding to the surface current shown by *black arrows* (February 7, 2001). Radar location (*black triangle*) and isobath 2,500 m (*black line*) are shown.

The second vortex (V2) is less easily detected, especially on RD and OD maps, because of its deviation from the theoretical model. In this case, the observation of a possible vortex on V_r is hardly confirmed on the other two quantities.

According to the detection quality indices defined in Sect. 2.1.2, very good detection is achieved (S=6) for 25% of the data set (e.g., V1 on Fig.5), and 40% are detected with acceptable confidence ($3<S<6$). Other cases are ambiguous (e.g., V2 where $\{r_{Vr}, r_{RD}, r_{OD}\}=\{1, 1, 1\}$).

The concomitant use of the V_r, RD, OD vortex patterns is necessary to certify the vortex existence. The VIM robustness is highly dependent on the symmetry properties of the structure. First, the closer the structure to a circular shape, the better its detection in V_r, RD, and OD maps. Second, the detection is optimal for a homogeneous distribution of the current intensity, which is generally not the case, e.g., when a vortex edge coincides with a boundary of the NC.

4 Application to experimental data

The VRM and the VIM techniques are now applied to measured data from HF/VHF radar campaigns. The most suitable data set is used for each method according to its performance requirements in terms of radar coverage or eddy occurrence.

4.1 Vectorial Reconstruction Method in the Gulf of La Spezia

Region 2 is chosen to test the VRM in real conditions. Data from radar 1 (Fig. 6a) are used to reconstruct the vector field according to its favorable implementation. The VRM characteristic curves are circles starting from the eastern side of the observation cone. The method's performance is evaluated by comparison with the current field resulting from the combination of the radial current maps from radar 1 and radar 2 (Fig. 6a).

An example of the current field computed from both radars is given in Fig. 6a, superimposed to the SCD for the error evaluation of the reconstruction method. Note that full surface currents and their divergence are not available everywhere in the observation cone of radar 1 due to the limited eastward extension of the coverage of radar 2. The SCD values are affected by the geometric dilution of precision (GDOP) of the zonal and meridional current components (e.g., Chapman et al. 1997; Shay et al. 2007). Since resulting uncertainties on SCD values were too high, radial data were smoothed spatially, and vector currents were reprocessed from these new data. Smoothing consisted in a 3-point running window giving an effective accuracy on radial current components of $\delta V_{r,\,\mathrm{eff}} \sim 0.6\times\delta V_r = 0.01\ \mathrm{ms}^{-1}$. The resulting SCD accuracy is shown on the same figure.

Vector speed differences (Eq. 9) between original and reconstructed current fields are shown in Fig. 6b. Only a limited area near the east coast presents relatively low VSD values (typically $<2\delta V_{r,\,\mathrm{eff}}$). Differences are important and can exceed $10\delta V_{r,\,\mathrm{eff}}$ at the western and southeastern parts of the computation grid. Variations of VSD, SCD, and $\mathrm{SCD_{cum}}$ values along a characteristic curve are given in Fig. 6c. As for the model data (Sect. 3.1), the VSD varies similarly to the absolute value of the $\mathrm{SCD_{cum}}$.

In the example shown in Fig. 6 and nearly for the entire experimental period, the VRM method gives inaccurate results. The time average of the vector speed difference, <VSD>, was performed at each point over the experimen-

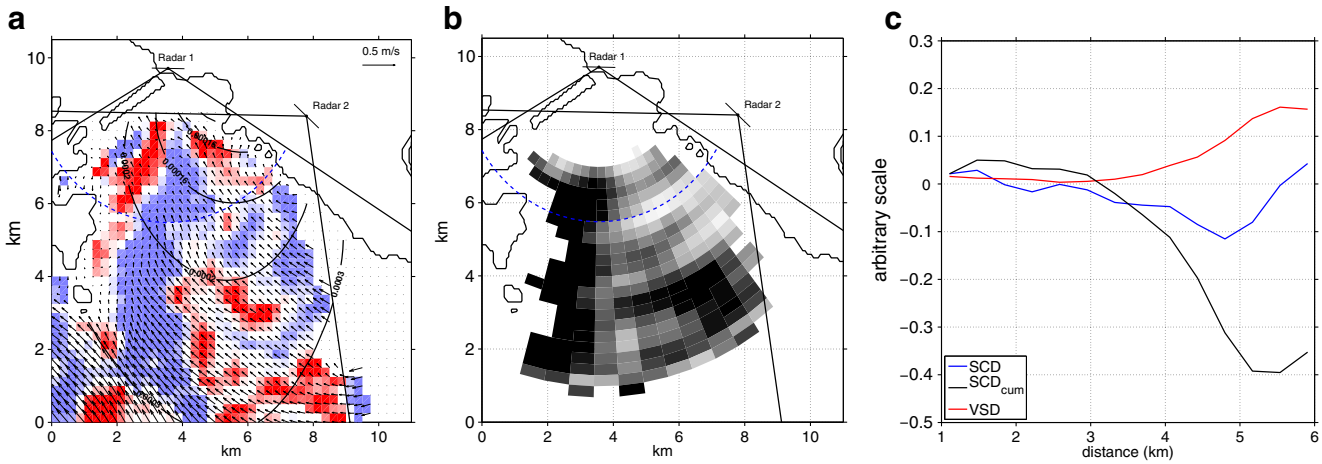

Fig. 6 **a** Radar-derived surface current field superimposed on SCD (*color bar*, -5.10^{-6} s^{-1} [*blue*] to 5.10^{-6} s^{-1} [*red*]); *black lines* represent SCD accuracy (per second). **b** Norm of VSD between reconstructed and original fields (0 ms^{-1} [*white*] to 0.1 ms^{-1} [*black*]). **c** Variation with distance along *dashed blue characteristic curve* of SCD×10^3 (per second) (*blue*), SCD_{cum}×10^3 (per second) (*black*), and VSD (meters per second) (*red*). The date is June 22, 2007, 1.30 a.m.

tal period (Fig. 7). <VSD> increases perpendicularly from the coast north of y=4 km and in the westward direction for smaller ordinates. This could be explained by the fact that characteristic curves cross regions of divergence that vary both in time and space. The difference between upper and lower regions seems to reflect some meridional heterogeneity of the SCD distribution along the east coast. Note that we can only suggest such interpretation due to the lack of vector data along the southeast coast.

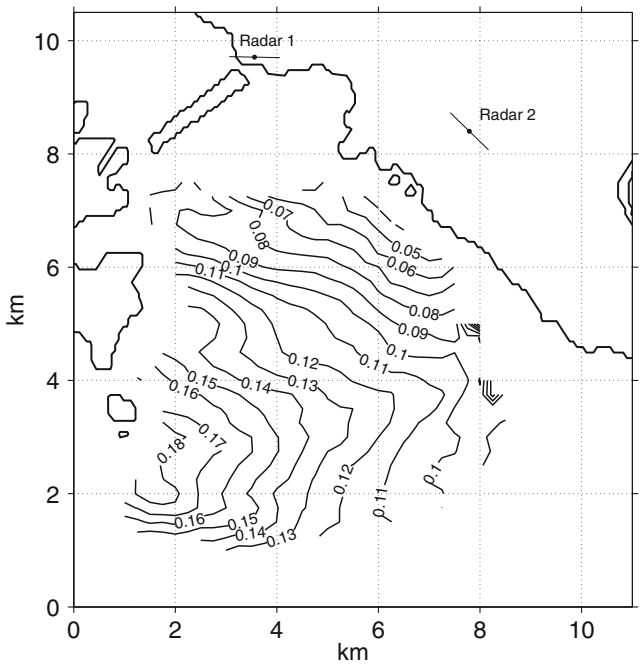

Fig. 7 Time average of vector speed difference norm (<VSD>) between VHF and reconstructed surface current (meters per second) over the experimental period (June 17–25, 2007)

<VSD> values are always greater than the errors on zonal and meridional current components due to the GDOP. Errors are defined here as the product of δV_r and GDOP values. For example, this error is lower than 0.015 ms^{-1} for ordinates greater than 5 km, whereas <VSD> is generally greater than 0.04 ms^{-1}.

While the required radar implantation for the use of the VRM is satisfied in region 2, the results are not satisfactory. The particular coastal zone of the Gulf of La Spezia reveals important divergence values altering the reconstruction and resulting in possible unrealistic features in the reconstructed field. Such properties could be assessed by numerical simulations. However, such a small and shallow basin is very difficult to model using a traditional hydrostatic Ocean General Circulation Model. The resolution of the available simulations during the MREA program is too coarse, resulting in an insufficiently accurate circulation (Haza et al. 2010).

4.2 Vortex Identification Method in the Gulf of Lions

The ECOLO campaign evidenced about 30 eddies in region 1 during the 1.5-year observational period (Allou et al. 2010; Schaeffer et al. 2011). The VIM was applied to the radial data from the northern radar (radar 2, Fig. 8) for each period where a vortex was evidenced in the current vector map resulting from the combination of the radial current maps from radar 1 and radar 2. Radar 2 was preferred to radar 1 (eastern radar) because of its better performances in terms of range and azimuth coverage. Data are available on an hourly basis.

Figure 8 gives a typical example of a vortex event, with indices $\{r_{Vr}, r_{RD}, r_{OD}\}=\{2, 1, 2\}$. It illustrates the influence

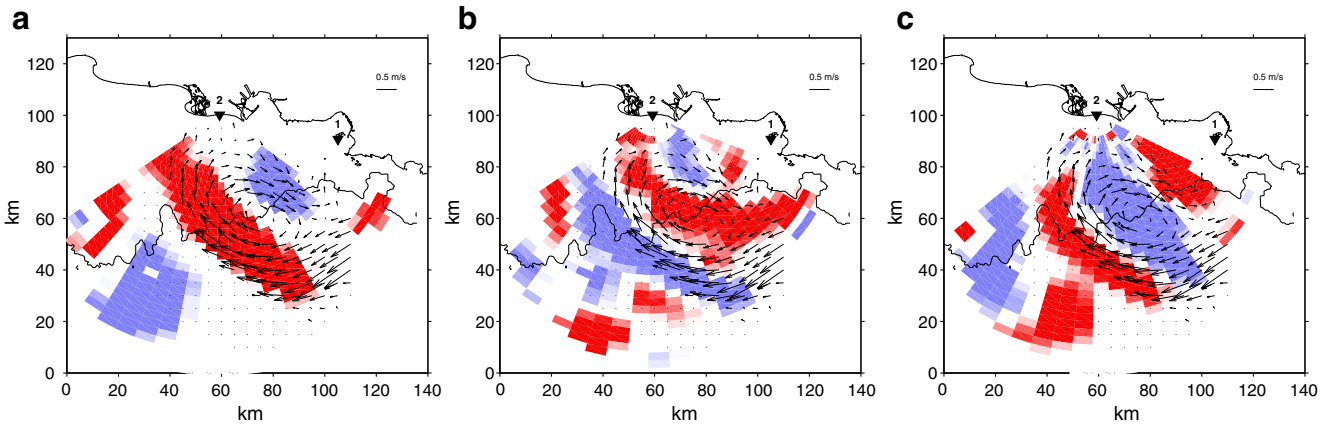

Fig. 8 VIM detection method applied to December 30, 2006, 6 p.m. Maps of **a** radial velocity field *Vr*, **b** radial derivative RD, and **c** orthoradial derivative OD of *Vr*. *Arrows* are surface current. *Black triangles* are radar locations. Isobath 130 m is drawn

of the current heterogeneity within the vortex, with currents higher at its southern boundary. This heterogeneity is due to the NC influence.

In most cases, it was possible to identify the vortices with the VIM method. Since vortices have a relative long lifetime, up to 50 h, detection ambiguities could be improved by considering the time evolution of radial maps. Using the same ranking of detection quality described in Sect. 2.1.2, the percentage of well-identified vortices is 81%. Moreover, S=6 is obtained for one third of them.

4.3 Vortex Identification Method along the Provence coasts

The VIM method is applied to the ECCOP campaign (region 3) where only one radar is running. This temporary limitation has strongly motivated the present study. We examined the radial data acquired every 30 min from July 29 to October 6, 2010. Applying the VIM requires a minimum area of valid data within the radar coverage. This area must be at least of the order of the vortex size. Hence, we only selected radar maps presenting coverage of valid data consistent with a vortex diameter of 50 km. Using this criterion and due to the actual quality of the data, only two thirds of the available radial maps could be used for the analysis (nearly 2,000 over 3,000 times).

Among this significant data set, we detected only three well-identified vortex events (August 19 (1), 21 (2), and September 13 (3), 2010; Fig. 9). They are observed both on V_r, RD, and OD fields (see for example Fig. 10 corresponding to event 2). Contrary to the ECOLO and MREA campaigns, no ground truth of surface current is available for validation. However, the results obtained both on modeled (region 3, Sect. 3.2) and experimental (region 1, Sect. 4.2) data allow us to be confident in the identification of these eddy-like structures. These three events represent a minimal estimation of eddy occurrence in the area because of missing data (as referred above) and partial inclusion of vortices within the radar coverage. However, this number remains rather small indicating a low eddy activity during the summer period. Despite the fact that numerical simulations are not yet available for the period studied, such seasonal minimum of eddy activity is qualitatively supported by our modeling

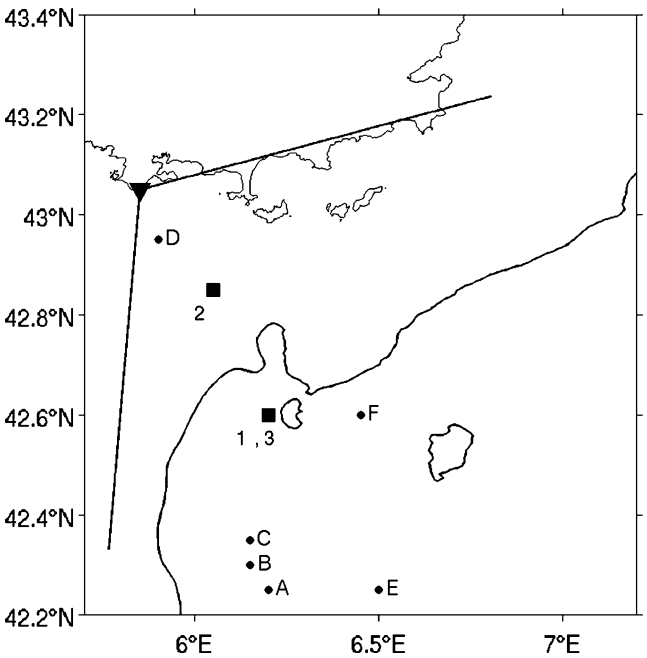

Fig. 9 Location of the three eddy events identified from VIM (*square numbers 1–3*) from experimental data spanning July 29–October 6, 2010. Points (*A–F*) mark the locations of eddy events observed on modeled data for the same period in 2001. The *cone* represents the azimuthal radar coverage, and the *black triangle* is the radar location. Isobath 2,500 m is drawn

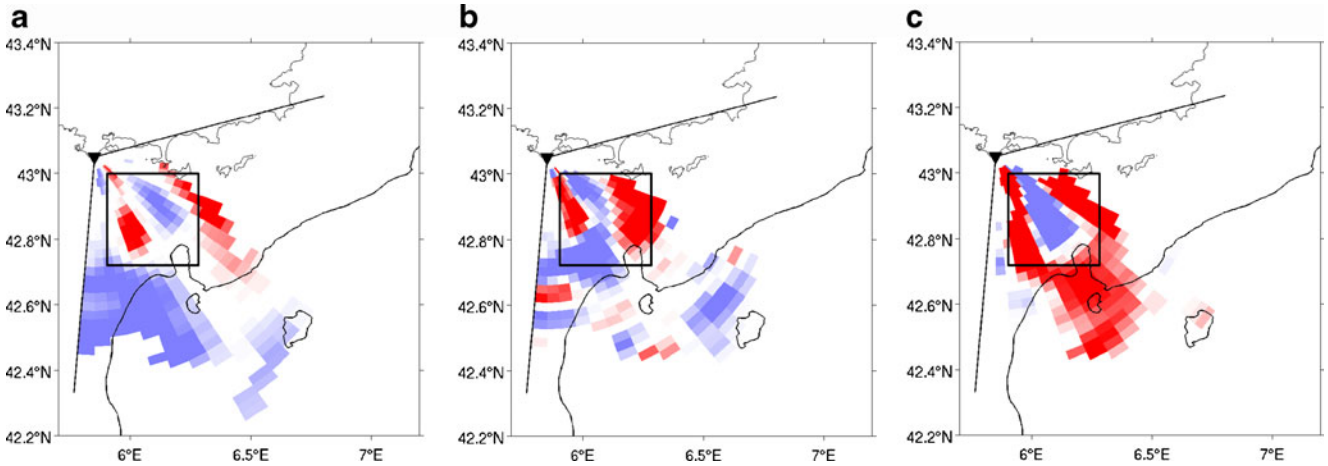

Fig. 10 **a** Radial velocity field V_r, **b** radial derivative RD, and **c** orthoradial derivative OD of V_r from experimental data of August 21, 2010. The vortex (*number 2* in Fig. 9) lies inside the *black rectangle*. The *cone* represents the azimuthal radar coverage, and the *black triangle* is the radar location. Isobath 2,500 m is drawn

results of 2001 (Sect. 3.2). Figure 9 reports the location of eddies observed in 2001 simulations (points A–F) for the same period of the year as the 2010 radar experiment (points 1–3). If we exclude the four southern eddies which are partly located outside the effective radar coverage for the data considered (lower than 80 km), the number and size (15–25 km) of eddies from radar and model data are similar.

5 Conclusion

In many circumstances, monitoring surface circulation in the coastal zone by HF/VHF radar can be hindered by the lack of data from one station (e.g., failure, interferences) or by logistic constraints that prevent, at least for a moment, implementation of a complete radar network. In these cases, radial current components are only available from one station. This paper aims at assessing two basic methods to get useful information on the current vector field from such scalar data.

The VRM method relies on the assumption of non-divergent horizontal surface flow and consists in computing the stream function along characteristic curves which coincide to range distances of the radar. A limiting constraint of the method for radar implementation is that it necessitates that one edge of the radar coverage intersects the land. The method was applied to radial current components produced by a hydrodynamic model and to observed data acquired with VHF radars. Due to the strong hypothesis of the method requesting a divergence-free field, the reconstructed currents can be inaccurate due to divergence properties of the zones. In fact, the VRM can only work in regions satisfying specific divergence properties, namely the cumulative divergence value along characteristic curves must be null. The selection of coastal ocean regions having these given properties could be determined from statistical analysis of the model data, allowing an a priori knowledge of the method pertinence.

The VIM does not rely on any physical assumption. The method aims at detecting eddy-like structures by the combined analysis of radial velocity and its derivatives. The method was developed using a theoretical vortex with circular symmetry and azimuthal homogeneity. We did not address the inversion problem. Hence, the VIM method in its present implementation is not intended to accurately reproduce the vortex but rather to identify its existence within a range of confidence and to give rough estimates of its position and size. The VIM succeeded to detect nearly all the eddies that were observed during a HF campaign in the Gulf of Lions and to detect eddy-like structures from a recent single site campaign along the Provence coasts area.

The question of making use of single radial maps was shown to be very challenging. Both methods presented here were successful in the theoretical case, satisfactory when using numerical model output, and less efficient when applied to real cases. The divergence-free hypothesis should be verified before the use of the VRM, and only well-pronounced eddies can be identified with the VIM. In spite of these constraints, the asset of these methods lies in their simplicity of implementation, quickly producing a first guess velocity field.

Another potential way to make use of radial current components, including the single radar case, is through data assimilation (e.g., recently Barth et al. 2008, 2010; Shulman and Paduan 2008). The increase of the Mediterranean observatory systems will certainly enhance the combined use of model and radial maps.

Acknowledgments ECCOP experiment is supported by LEFE/IDAO (CNRS/INSU), Med Program (TOSCA 2G-MED09-425), and GIRAC Pôle Mer. We acknowledge the support of MREA/LASIE and POET experiments. We are pleased to acknowledge Yves Barbin and Joel Gaggelli for their major contribution to radar field campaigns of this study. We are grateful to Yann Ourmières for his careful reading of the paper.

References

Allou A, Forget P, Devenon J-L (2010) Submesoscale vortex structures at the entrance of the Gulf of Lions in the Northwestern Mediterranean Sea. Cont Shelf Res 30:724–732

André G, Garreau P, Garnier V, Fraunié P (2005) Modelled variability of the sea surface circulation in the North-western Mediterranean Sea and in the Gulf of Lions. Ocean Dynamics 55:294–308

Barth A, Alvera-Azcarate A, Weisberg RH (2008) Assimilation of high-frequency radar currents in a nested model of the West Florida Shelf. J Geophys Res 113:C08033. doi:10.1029/2007JC004585

Barth A, Alvera-Azcarate A, Gurgel K-W, Staneva J, Port A, Beckers J-M, Stanev EV (2010) Ensemble perturbation smoother for optimizing tidal boundary conditions by assimilation of High-Frequency radar surface currents - application to the German Bight. Ocean Sci 6(1):161–178. doi:10.5194/os-6-161-2010

Béranger K, Drillet Y, Houssais M-N, Testor P, Bourdallé-Badie R, Alhammoud B, Bozec A, Mortier L, Bouruet-Aubertot P, Crépon M (2010) Impact of the spatial distribution of the atmospheric forcing on water mass formation in the Mediterranean Sea. J Geophys Res 115:C12041. doi:10.1029/2009JC005648

Chapman RD, Shay LK, Graber HC, Edson JB, Karachintsev A, Trump CL, Ross DB (1997) On the accuracy of HF radar surface current measurements: intercomparisons with ship-based sensors. J Geophys Res 102:18737–18748

Crombie DD (1955) Doppler spectrum of sea echo at 13.56 Mc/s. Nature 175:681–682

Estournel C, de Madron Durrieu X, Marsaleix P, Auclair F, Julliand C, Vehil R (2003) Observation and modelisation of the winter coastal oceanic circulation in the Gulf of Lions under wind conditions influenced by the continental orography (FETCH experiment). J Geophys Res 108(C3):7.1–7.18

Flexas MM, Durrieu de Madron X, Garcia MA, Canals M, Arnau PA (2002) Flow variability in the Gulf of Lions during the MATER HFF experiment (March–May 1997). J Mar Syst 33–34:197–214

Forget P, Barbin Y, André G (2008) Monitoring of surface ocean circulation in the Gulf of Lion (North-West Mediterranean Sea) using WERA HF radars. Proceedings IGARSS 2008, Boston, USA, 7–11 Juillet 2008

Frisch AS, Leise J (1981) A note on using continuity to extend HF radar surface-current measurements. J Geophys Res 86:11089–11090

Gurgel KW, Antonischki G, Essen HH, Schlick T (1999) WEllen RAdar (WERA), a new ground-wave based HF radar for ocean remote sensing. Coastal Eng 37:219–234

Haza A, Ozgokmen TM, Griffa A, Molcard A, Poulain P-M, Peggion G (2010) Transport properties in small scale coastal flows: relative dispersion from VHF radar measurements in the Gulf of La Spezia. Ocean Dynamics 60(4):861–882

Hu ZY, Doglioli AM, Petrenko AA, Marsaleix P, Dekeyser I (2009) Numerical simulation of mesoscale eddies in the Gulf of Lion. Ocean Modelling 20:203–208

Hu ZY, Petrenko AA, Doglioli AM, et al. (2011) Study of coastal eddies: application in the Gulf of Lion. J. Marine Syst., (in press)

Hua B, Thomasset F (1983) A numerical study of the effects of coastline geometry on wind-induced upwelling in the Gulf of Lions. J Phys Oceanogr 13:678–694

Jacob D, Andrae U, Elgered G, Fortelius C, Graham LP, Jackson SD, Karstens U, Koephen C, Lindau R, Podzun R, Rockel B, Rubel F, Sass HB, Smith RND, Van den Hurk BJJM, Yang X (2001) A comprehensive model intercomparison study investigating the water budget during the BALTEXPIDCAP period. Meteorol Atmops Phys 77(1–4):19–43

Kaplan DM, Largier J (2006) HF radar-derived origin and destination of surface waters off Bodega Bay, California. Deep-Sea Res 53:2906–2930

Kaplan DM, Lekien F (2007) Spatial interpolation and filtering of surface current data based on open-boundary modal analysis. J Geophys Res 112:C12007. doi:10.129/2006JC003984

Kim SY (2010) Observations of submesoscale eddies using high-frequency radar-derived kinematic and dynamic quantities. Cont Shelf Res 30:1639–1655

Langlais C, Barnier B, Molines JM, Fraunié P, Jacob D, Kotlarski S (2009) Evaluation of a dynamically downscaled atmospheric réanalyse in the prospect of forcing long term simulations of the ocean circulation in the Gulf of Lions. Ocean Modelling 30:270–286

Large WG, Yeager SG (2004) Diurnal to decadal global forcing for ocean and sea ice models: the data sets and flux climatologies. Climate and Global Dynamics Division, Colorado, NCAR technical note

Leise JA (1984) The analysis and digital signal processing of NOAA's surface current mapping system. IEEE L Oceanic Eng 9(2):106–113

Lekien F, Coulliette C, Bank R, Marsden J (2004) Open-boundary modal analysis: interpolation, extrapolation, and filtering. J Geophys Res 109:C12004. doi:10.1029/2004JC002323

Lipa BJ (2003) Uncertainties in SeaSonde current velocities. In: Proceedings of the IEE/OES Seventh Working Conference on Current Measurement Technology, San Diego CA, pp. 95–100

Lipa BJ, Barrick DE (1983) Least-squares methods for the extraction of surface currents from CODAR crossedloop data: application at ARSLOE. IEEE J Oceanic Eng 8(4):226–253

Lipa BJ, Nyden B, Ullman DS, Terill E (2006) SeaSonde radial velocities: derivation and internal consistency. IEEE J Oceanic Eng 31(4):850–861

Lipphardt BL, Kirwan AD, Grosch CE, Lewis JK, Paduan JD (2000) Blending HF radar and model velocities in Monterey Bay through normal mode analysis. J Geophys Res 105(C2):3425–3450

Liu L, Wu X, Cheng F, Yang S, Ke H (2007) Algorithm for HF radar vector current measurement. J Oceanogr 63:47–66

Madec G (2008) NEMO ocean general circulation model reference manual. Internal report. LODYC/IPSL, Paris

Martin AP, Richards KJ, Law CS, Liddicoat M (2001) Horizontal dispersion within an anticyclonic mesoscale eddy. Deep-Sea Res 48:739–755

May PT, Weber BL, Strauch RG, Lataitis RJ, Moran KP, Meritt DA (1989) Single station ocean current vector measurement: application of the spaced antenna (SA) technique. Geophys Res Lett 16(9):999–1002. doi:10.1029/GL016i009p00999

Millot C (1990) The Gulf of Lions' hydrodynamics. Cont Shelf Res 10 (9–11):885–894

Millot C (1999) Circulation in the Western Mediterranean Sea. J Mar Syst 20:423–442

Molcard A, Poulain PM, Forget P, Griffa A, Barbin Y, Gaggelli J, De Maistre JC, Rixen M (2009) Comparison between VHF radar observations and data from drifter clusters in the Gulf of La Spezia (Mediterranean Sea). J Mar Syst 78(S1):S79–S89

Ourmières Y, Zakardjian B, Beranger K et al. (2011) Assessment of a NEMO-based downscaling experiment for the North-Western Mediterranean region: impacts on the Northern Current and comparison with ADCP data and altimetry products. Ocean Modelling (in press)

Parks AB, Shay LK, Johns WE, Martinez-Pedraja J, Gurgel K-W (2009) HF radar observations of small-scale surface current variability in the Straits of Florida. J Geophys Res 114:C08002. doi:10.1029/2008JC005025

Petrenko AA (2003) Variability of circulation features in the Gulf of Lion NW Mediterranean Sea. Importance of inertial currents. Oceanologica Acta 26:323–338

Petrenko A, Leredde Y, Marsaleix P (2005) Circulation in a stratified and wind-forced Gulf of Lions, NW Mediterranean Sea: in situ and modeling data. Cont Shelf Res 25:7–27

Rixen M, Book JW, Orlic M (2009) Coastal processes: challenges for monitoring and prediction. J Mar Sys 78:S1–S2

Sammari C, Millot C, Prieur L (1995) Some aspects of the seasonal and mesoscale variabilities of the Northern Current inferred from the PROLIG-2 and PROS-6 experiments. Deep-Sea Res 42 (6):893–917

Schaeffer A, Molcard A, Forget P, et al. (2011) Generation mechanism of mesoscale eddy in the Gulf of Lions: radar observation and modelling. Ocean Dynam (in press)

Schmidt RO (1986) Multiple emitter location and signal parameter estimation. IEEE Trans Antennas Propag AP-34(3):276–280

Sentchev A, Forget P, Barbin Y (2009) Residual and tidal circulation revealed by VHF radar surface current measurements in the southern Channel Isles region (English Channel). Estuarine, Coastal and Shelf Sci 82:180–192

Shadden SC, Lekien F, Paduan JD, Chavez FP, Marsden JE (2009) The correlation between surface drifters and coherent structures based on high-frequency radar data in Monterey Bay. Deep Sea Res II 56:161–172

Shay KL, Martinez-Pedraja J, Cook TM, Haus BK, Weisberg RH (2007) High-frequency radar mapping of surface currents using WERA. J Atmos Ocean Technol 24:484–503

Shulman I, Paduan JD (2008) Assimilation of HF radar-derived radials and total currents in the Monterey Bay area. Deep-Sea Res 56:149–160. doi:10.1016/j.dsr2.2008.08.004

Stewart RH, Joy JW (1974) HF radio measurements of surface currents. Deep Sea Res 21:1039–1049

Yaremchuk M, Sentchev A (2009) Mapping radar-derived sea surface currents with a variational method. Cont Shelf Res 29:1711–1722

Yoshikawa Y, Matsuno T, Marubayashi K, Fukudome K (2007) A surface velocity spiral observed with ADCP and HF radar in the Tsushima Strait. J Geophys Res 112:C06022. doi:10.1029/2006JC003625